

Experimental observation of front propagation in LL model with negative diffractive and inhomogeneous Kerr cavity

V. Odent¹, M. Tlidi¹, M.G. Clerc², and E. Louvergneaux¹

¹ *Laboratoire de Physique des Lasers, Atomes et Molécules, CNRS UMR8523, Université Lille 1, 59655 Villeneuve d'Ascq Cedex, France*

² *Faculté des Sciences, Université libre de Bruxelles (U.L.B.), C.P. 231, Campus Plaine, B-1050 Bruxelles, Belgium and*

³ *Departamento de Física, Universidad de Chile, Blanco Encalada 2008, Santiago, Chile*

A driven resonator with focusing Kerr nonlinearity shows stable localized structures in a region far from modulational instability. The stabilization mechanism is based on front interaction in bistable regime with an inhomogeneous injected field. The experimental setup consist of a focusing Kerr resonator filled with a liquid crystal and operates in negative optical diffraction regime. Engineering diffraction is an appealing challenging topic in relation with left-handed materials. We solve the visible range of current left-handed materials to show that localized structures in a focusing Kerr Fabry-Perot cavity submitted to negative optical feedback are propagating fronts between two stable states. We evidenced analytically, numerically, and experimentally that these fronts stop due to the spatial inhomogeneity induced by the laser Gaussian forcing, which changes spatially the relativity stability between the connected states.

PACS numbers:

I. INTRODUCTION

Localized structures (LS's) often called cavity solitons in dissipative media have been observed in various fields of nonlinear science (see last overview on this issue [1–3]). Localized structures consist of isolated or randomly distributed peaks surrounded by regions in the homogeneous steady state. Currently they attract growing interest in optics due to potential applications for all-optical control of light, optical storage, and information processing. They appear in an optical resonator containing a third order nonlinear media such as liquid crystals, and driven coherently by an injected beam in a positive diffraction regime and close to modulational instability [4, 5]. The existence of localized structures and localized patterns, due to the occurrence of a modulational instability, has been abundantly discussed and is by now fairly well understood [6]. In this case, LS's appears in the subcritical modulational instability regime where there is a coexistence between the homogeneous steady state and the spatially periodic pattern. Localized structures consist of isolated or randomly distributed spots surrounded by regions in the uniform state. They may consist of peaks or dips embedded in the homogeneous background.

However, localized structures could be formed in modulationally stable regime [7]. In this case, heterogeneous initial conditions usually caused by the inherent fluctuations generate spatial domains, which are separated by their respective interfaces often called front solutions or interfaces or domain walls [8]. Interfaces between these metastable states appear in the form of propagating fronts and give rise to a rich spatiotemporal dynamics [9, 10]. From the point of view of dynamical system theory at least in one spatial dimension a front is a nonlinear solution that is identified in the comoving frame system as a heteroclinic orbit linking two spatially extended states [11, 12]. The dynamics of the interface depends on the nature of the states that are connected. In the case of a front connecting a stable and an unstable state, it is called as Fisher-Kolmogorov-Petrovsky-Piskunov (FKPP) front [13–16]. One of the characteristic features of these fronts is that the speed is not unique, nonetheless determined by the initial conditions. When the initial condition is bounded, after a transient, two counter propagative fronts with the minimum asymptotic speed emerge [13, 16]. In case that the nonlinearities are weak, this minimum speed is determined by the linear or marginal-stability criterion and fronts are usually referred to as pulled [16]. In the opposite case, the asymptotic speed can only be determined by nonlinear methods and fronts are referred to as pushed [16]. The above scenario changes completely for a front connecting two stable states. In the case of two uniform states, a gradient system tends to develop the most stable state, in order to minimize its energy, so that the front always propagates toward the most energetically favored state [17]. It exists only as one point in parameter space for which the front is motionless, which is usually called the Maxwell point, and is the point for which the two states have exactly the same energy for variational systems [18].

In this chapter, we present analytical, numerical and experimental investigation of of front interaction in bistable regime with an inhomogeneous injected beam. Far from any modulational instability, the inhomogeneous injected beam in the form of Gaussian, can lead to the stabilization of LS's. This completes our previous communication of the stability of LS's [19]. We consider an experimental setup which consists of a focusing Kerr resonator filled with a

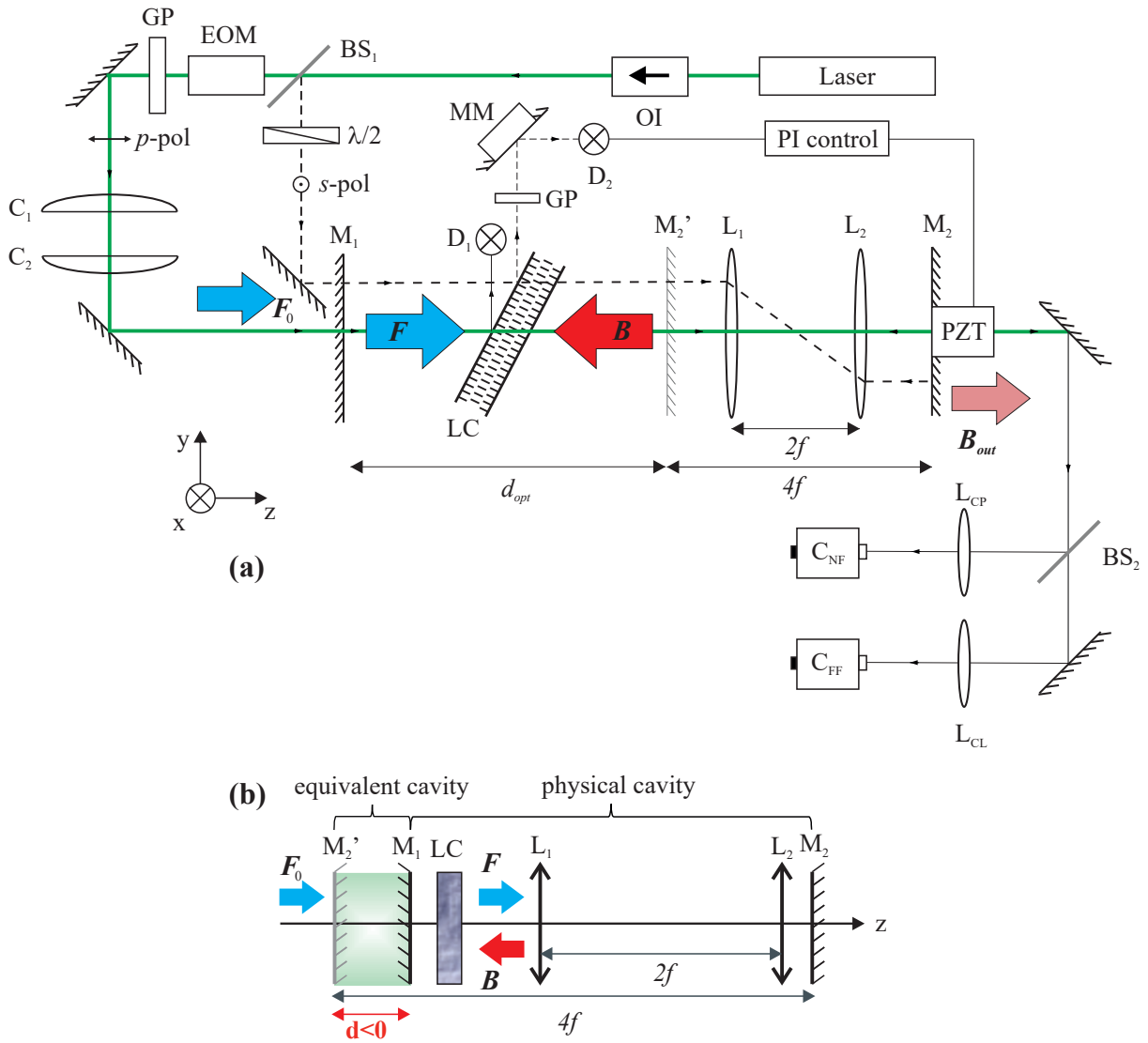


Figure 1: Inhomogeneous Kerr cavity with negative diffraction: (a) Experimental setup. (b) Schematic representation of the physical cavity and the equivalent cavity, with negative cavity length. OI optical isolator; BS beam splitter; EOM electro-optical modulator; GP Glan polarizer; C_1 and C_1 cylindrical lenses; LC liquid crystal slice; D₁ and D₂ photodetectors; MM motorized mirror; L₁ and L₂ lenses of focal length f : p and s are the polarized components of the pump (solid line) and probe (dashed line) beams respectively; C_{NF} and C_{FF} near field and far field cameras; M₁ and M₂ are the real cavity mirrors but the optical Perot-Fabry cavity is delimited by M₁ and M'₂ mirrors and its length is d .

liquid crystal and operates in negative optical diffraction regime. Engineering diffraction is an appealing challenging topic in relation with left-handed materials. We solve the visible range of current left-handed materials [20–22, 24] to show that LS's in a focusing Kerr Fabry-Perot cavity submitted to negative optical feedback are propagating fronts between two stable states. Moreover, we have evidenced that these fronts stop due to the spatial inhomogeneity induced by the laser Gaussian forcing, which changes spatially the relativity stability between the connected states.

This chapter is organized as follows. After an introduction we present the experimental setup and experimental observation in Sec. 2. The analytical and numerical investigations are presented in Sec 3. The special case with a null diffraction is developed in Sec. 4. We conclude in Sec. 5.

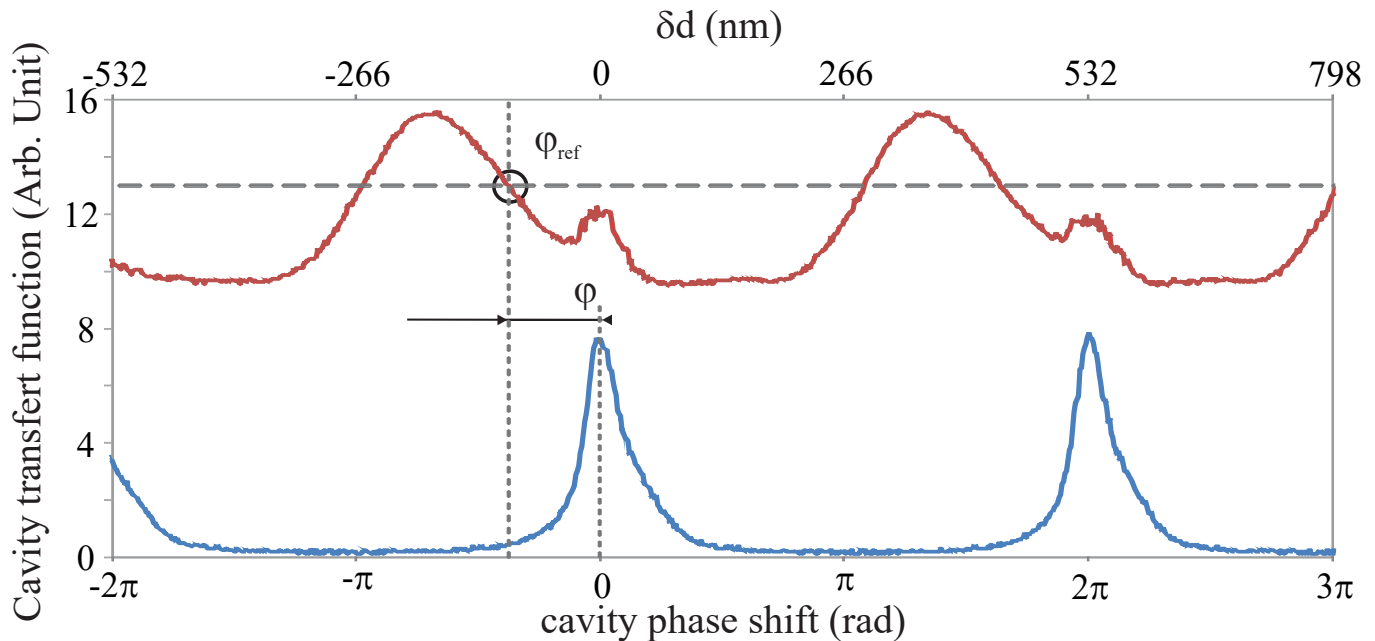


Figure 2: Transfer function of the optical cavity for : pump beam (blue line) and probe beam (red line). φ linear phase shift of the cavity. δd cavity length variation.

II. EXPERIMENTAL

A. Set-up

The experiments have been carried out using a nonlinear Kerr slice medium inserted in an optical Fabry-Perot resonator. The Kerr focusing medium is a $50\text{-}\mu\text{m}$ -thick layer of E7 nematic liquid crystal homeotropically anchored. Two plane mirrors M_1 and M_2 define the physical cavity but the optical one is delimited by M_1 and M'_2 (which is the image of M_2 through the $4f$ lens arrangement) and its optical length is d [Fig. 1]. The intensity reflexion coefficients of M_1 and M_2 mirrors are $R_1 = 81.4$ and $R_2 = 81.8$ respectively so that the cavity finesse is estimated to 15. The experimental recording of the Airy function (blue curve) on Fig. 2 gives a finesse of 11.6 indicating the presence of supplementary losses due to nonlinear medium and lenses transmission coefficients.

The optical cavity length d may be tuned from positive to negative values [positive on Fig. 1(a) and negative on Fig. 1(b)]. Thus, for negative optical cavity path ($d < 0$), a beam propagating along this path experiences negative diffraction. Together with the positive Kerr index, the experimental setup is then equivalent to a Kerr cavity that would have a positive optical distance but negative Kerr index (the ηa product sign in Ref. [26] that defines the type of transverse instabilities remains the same). However the physical mechanisms of negative refraction and negative diffraction are different. Thus, this intra-cavity geometrical lens arrangement allows for achieving an equivalent left-handed Kerr material in the visible range. It also allows to continuously tune the diffraction from positive to negative.

The laser source used is a single mode frequency doubled $Nd^{3+}:\text{YVO}_4$ laser ($\lambda_0 = 532\text{ nm}$) at $5W$. We have split the laser beam into two parts, a pump beam containing 95% of the initial power and a probe beam with 5% of the initial power. The pump beam power is controlled by an electro-optical modulator associated with a Glan polarizer. Then it is shaped by means of two cylindrical telescopes. The resulting beam size ($\sim 200\ \mu\text{m} \times 2800\ \mu\text{m}$) gives a "cigar" transverse shape such that only one spot can develop in one of the two directions. This beam is injected inside the cavity may then be considered as one-dimensional. The probe beam polarization is rotated to 90° to prevent interference phenomenon inside the cavity between the two beams (see Fig. (1)) The pump beam propagating in the forward direction is monitored at the output of M_2 mirror. We record the near field on C_{NF} and the far field on C_{FF} . The cavity detuning is an important parameter, because it determines the solution type (mono/bistable) of the cavity and also the energy quantity inside the cavity, as shown on the cavity transfer function on Fig. 2. For these reasons, we perform an active stabilization of the cavity phase shift, based on Coen's work and coworkers [25]. We stabilize the cavity length around a reference phase on the beam probe (φ_{ref} on Fig. 2), then we measure the phase shift between the probe and the pump beams to have the real cavity detuning φ , as presented on Fig. (2). Our setup

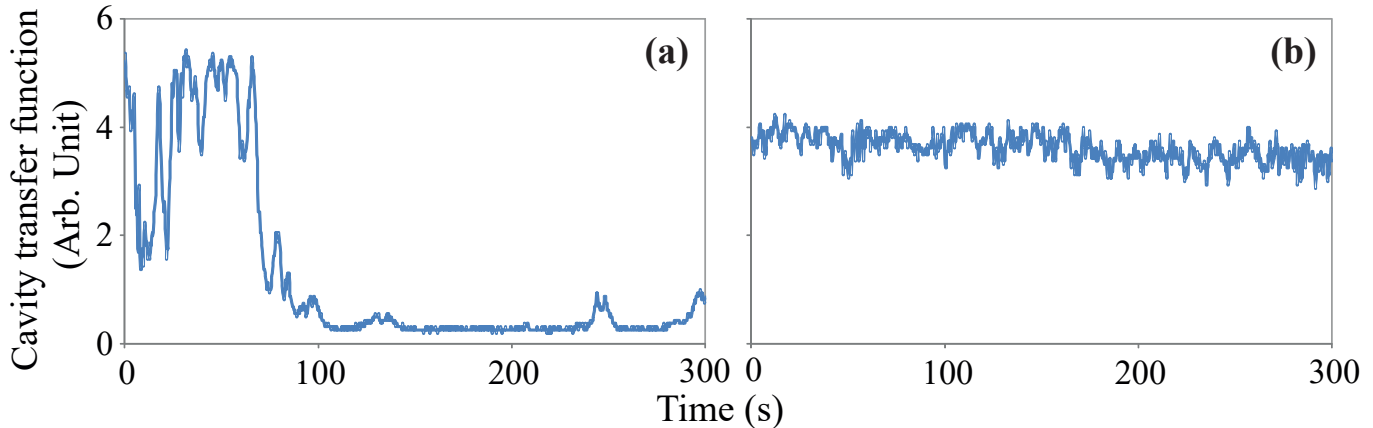


Figure 3: Temporal evolution of cavity transfer function correlated to cavity phase shift: (a) without stabilization; (b) with stabilization. $d = 5 \text{ mm}$, $I = 37 \text{ W/cm}^2$.

allow to maintain the detuning long enough to realize experiments, it means to have a fix value $\pm\pi/19$ during many minutes. Without the stabilization, the cavity detuning can evolve quickly and not permit us to do experiments. The typical detuning evolution without and with an active stabilization are presented on Fig. (3).

B. Experimental observations

As the input power is suddenly increased to the upper bistability response branch ($t = 0 \text{ s}$), the central part of transmitted intensity profile suddenly jumps after some latency time [$t \approx 37 \text{ s}$ on Fig. 4(c)] to a higher value and invades the surroundings towards the external regions where the field is less intense before stopping its propagation. Finally, the fronts locks to give a localized light state [Fig. 4(b)]. Changing the waist w of the Gaussian forcing or its intensity within the bistability region allows to tune the distance between the bounded fronts and so the localized state extension.

A transverse cut of the transmitted intensity profile is depicted on Fig. 4(a) obtained in the initial and the final observation period. This figure emphasizes the coexistence of different states in the same region of parameters. In addition, a state emerges from the other because of the inherent fluctuations of the system. Figure 4(c) shows this phenomenon starting at $t \approx 37 \text{ s}$. From this instant, the system exhibits two counter-propagating fronts, which will become asymptotically motionless [see Fig. 4(c)]. The motionless front is observed at the location $x_0(\text{expt}) \cong \pm 0.17w$. At this location, the input intensity is only 3 % lower than at the center of the input beam. Thus, we have observed experimentally coexistence between two inhomogeneous states, the noise induces a pair of fronts among these states, which initially are counter-propagate and asymptotically they stop.

III. ANALYTICAL RESULTS

A. Model equation

The dynamics of the single longitudinal mode of the bistable system which consist of a Fabry-Perot cavity filled with liquid crystal Kerr like medium and driven by a coherent plane-wave steady can be described by the simple partial differential equation (the LL model [26]) in which we incorporate an inhomogeneous injected field. This mean field approach model is valid under the following approximations: the cavity possess a high Fresnel number *i.e.*, large-aspect-ratio system and we assume that the cavity is much shorter than the diffraction and the nonlinearity spatial scales; and for the sake of simplicity, we assume a single longitudinal mode operation. Under these assumptions the space-time evolution of the intracavity field is described by the following partial differential equation

$$\frac{\partial E}{\partial t} = E_{in}(x) - (1 + i\Delta)E + i|E|^2E - i|\alpha| \frac{\partial^2 E}{\partial r^2} + \sqrt{\varepsilon}\xi(x, t) \quad (1)$$

which includes the effect of diffraction, which is proportional to α ; E is the normalized slowly-varying envelope of the electric field, Δ is the detuning parameter, E_{in} is the input field assumed to be real, positive and spatially

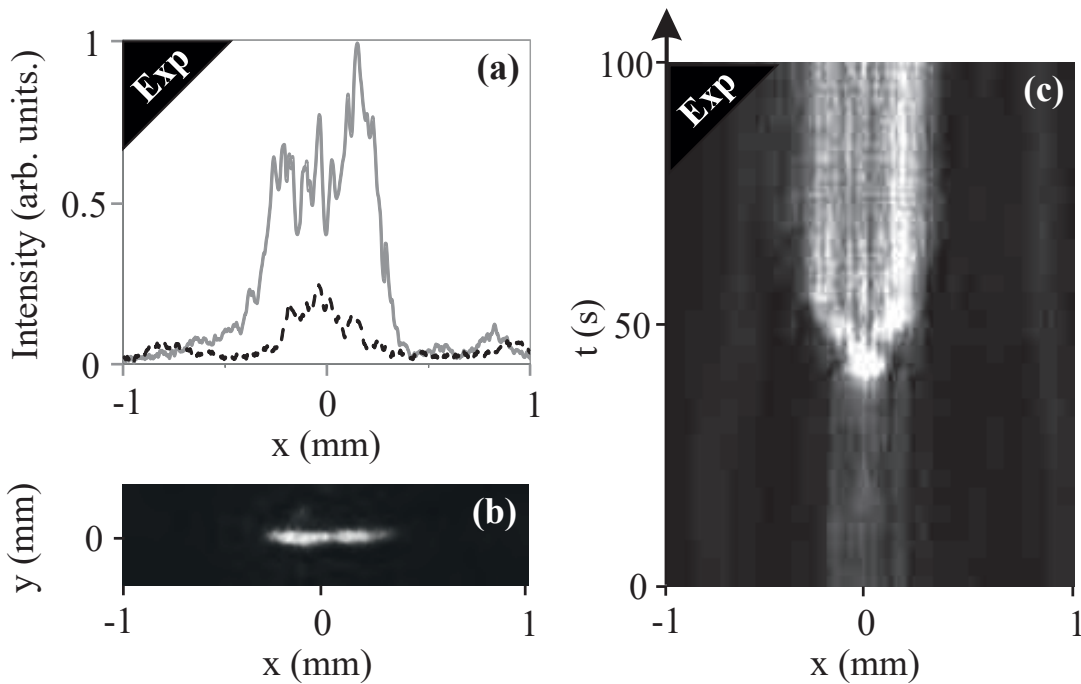


Figure 4: Experimental front propagation in negative diffractive inhomogeneous Kerr cavity. (a) Transverse cross-section of the initial (final) average localized structure in dashed black line (in continue gray line). (c) Spatiotemporal response to a step function of the input intensity from the lower to the upper branch of the bistable cycle. (b) cross section of the localized state. Light region account for high intensity of the light. $I_0 = 433 \text{ W.cm}^{-2}$, $d = -5 \text{ mm}$, $\varphi = -0.6 \text{ rad}$, $w_x = 1400 \mu\text{m}$, $w_y = 100 \mu\text{m}$, $R_1 = 81.8 \%$; $R_2 = 81.4 \%$.

inhomogeneous. The negative diffraction coefficient is $|\alpha|$. Note that the above model has been derived for a cavity filled with left-handed material operating in negative diffraction regime [21]. ε scales the noise amplitude and $\xi(x, t)$ are Gaussian stochastic processes of zero mean and delta correlation introduced to model thermal noise [27].

B. Derivation of F-KPP equation

The following development is realized for the deterministic case of Eq. 1 ($\varepsilon = 0$). The homogeneous steady states of Eq. (1) are solutions of $E_i = [1 + i(\Delta - |E_s|^2)]E_s$. The response curve involving the intracavity intensity $|E_s|^2$ as a function of the input intensity $|E_i|^2$ is monostable for $\Delta < \sqrt{3}$ and exhibits a bistable behavior when the detuning $\Delta > \sqrt{3}$. For $\Delta = \sqrt{3}$, we obtain the critical point associated with bistability where the output versus input characteristics have an infinite slope. At the critical point, the coordinate of the intracavity are $E_c = u_c + iv_c$ with $u_c = 3^{1/4}/\sqrt{2}$ and $v_c = -1/3^{1/4}\sqrt{2}$, and the injected field amplitude is $E_{in}^c = 2\sqrt{2}/3^{3/4}$.

The analytical investigation of fronts dynamics connecting two-homogeneous steady states in the framework of the Lugiato-Lefever model Eq. (1) is far from the scope of the present chapter. In this section we perform a derivation of a simple bistable model with inhomogeneous injection to study analytically the dynamics of the front connecting the two-homogeneous steady states. To do that, we introduce a small parameter that measures the distance from the critical point $\zeta \ll 1$ and we express the cavity detuning in the form

$$\Delta = \Delta_c(1 + \zeta^2\sigma) \quad (2)$$

where σ is a quantity of order one. Then, we decompose the envelope of the electric field into its real and imaginary parts: $E = x_1 + ix_2$ and we introduce a new space and time scales as $(x, t) \equiv (\zeta^2 t/\sigma, 3^{1/4}\zeta x/(\sqrt{\sigma}))$. The injected field can be expanded as

$$E_{in} = E_{in}^c \left(1 + \frac{3\zeta^2 I}{4} + \zeta^3 \alpha + \dots \right) \quad (3)$$

Let $(u, v) = (x_1, x_2) - (u_c, v_c)$ be the deviations of the real, the imaginary parts of intracavity field with respect to the values of these quantities at the critical point. Inserting these expansion into the LL model and using the above scalings, we obtain

$$\frac{\partial u}{\partial t} = \zeta \left(\frac{u^2}{2} + uv + \frac{v^2}{2} \right) + \zeta^2 \left(\frac{4\alpha}{3} - Iv + \frac{u^2 v}{2} + \frac{v^3}{6} \right) - \frac{1}{\sqrt{3}} \frac{\partial^2 v}{\partial x^2}, \quad (4)$$

$$\frac{\partial v}{\partial t} = -2(u + v) + \zeta \left(3I - \frac{9u^2}{2} - uv - \frac{v^2}{2} \right) + \frac{\zeta^2}{2} (6Iu - 3u^2 - uv^2) + \sqrt{3} \frac{\partial^2 u}{\partial x^2}. \quad (5)$$

Our aim is to seek solutions of Eqs. (4,5) in the neighborhood of the critical point associated with the optical bistability. To this end, we expand the cavity field and the injected field as

$$(u, v) = \zeta[(u_0, v_0) + \zeta(u_1, v_1) + \zeta^2(u_2, v_2) + \zeta^3(u_3, v_3) + \dots] \quad (6)$$

Inserting these expansions and taking into account of Eqs. (2,3) into the LL model and using the above scalings, we then obtain a hierarchy of linear problems for the unknown functions. At the first order in ζ , we find $u_0 = -v_0$. At the second, we have $v_1 = -u_1 + 3I/2 - u_0^2$. Finally, at the third order, we get a simple bistable model

$$\frac{\partial u}{\partial t} = f(u) + \frac{\partial^2 u}{\partial x^2} \quad (7)$$

where $u(x, t) = \sqrt{3/(2\sigma)}u_0$ is a scalar field that accounts for the real part of the envelope E ,

$$f(u) = \eta + u - u^3 \quad (8)$$

and $\eta = 4y_2\sigma/3$ controls the relative stability between the equilibria. Note that y_2 is proportional to the pumping E_{in} . Hence, if the pumping is inhomogeneous then the parameter η is also inhomogeneous. For a Gaussian pumping, we consider

$$\eta(x) \equiv \tilde{\eta} + \eta_0 e^{-(x/w)^2}, \quad (9)$$

where η_0 accounts for the strength of the spatial pumping beam and w is the width of the Gaussian. For $\eta(x) = 0$ both states are symmetric corresponding to the Maxwell point, where a front between these states is motionless.

To perform analytical developments, we use further approximation by taking into account only the first order development close to the center of the optical pumping where the stress is maximum, i.e.,

$$\eta(x) \approx -\tilde{\eta} + \eta_0 (1 - (x/w)^2) \quad (10)$$

close to the Maxwell point, one can consider the following ansatz for the front solution $u(x, t) = \tanh[(x - x_0(t))/\sqrt{2}] + H$, where x_0 is the front position and H accounts for small corrections. We substitute the above ansatz for $u(x, t)$ in Eq. (7), linearizing in H and imposing the solvability condition, we obtain the kinetic equation for the evolution of the front position

$$\dot{x}_0 = \frac{-3\sqrt{2}}{2} \left[-\tilde{\eta} + \eta_0 \left(1 - \left(\frac{x_0}{w} \right)^2 - \left(\frac{\pi}{\sqrt{6}w} \right)^2 \right) \right]. \quad (11)$$

this equation takes into account of corrections imputable to inhomogeneities of the injected signal. The stationary solutions of this equation reads

$$x_0 = \pm w \sqrt{1 - \frac{\tilde{\eta}}{\eta_0} - \frac{\pi^2}{6w^2}}, \quad (12)$$

the term $\pi^2/(6w)$ is negligible for w large. In this case, we have

$$x_0 = \pm w \sqrt{1 - \frac{\tilde{\eta}}{\eta_0}}. \quad (13)$$

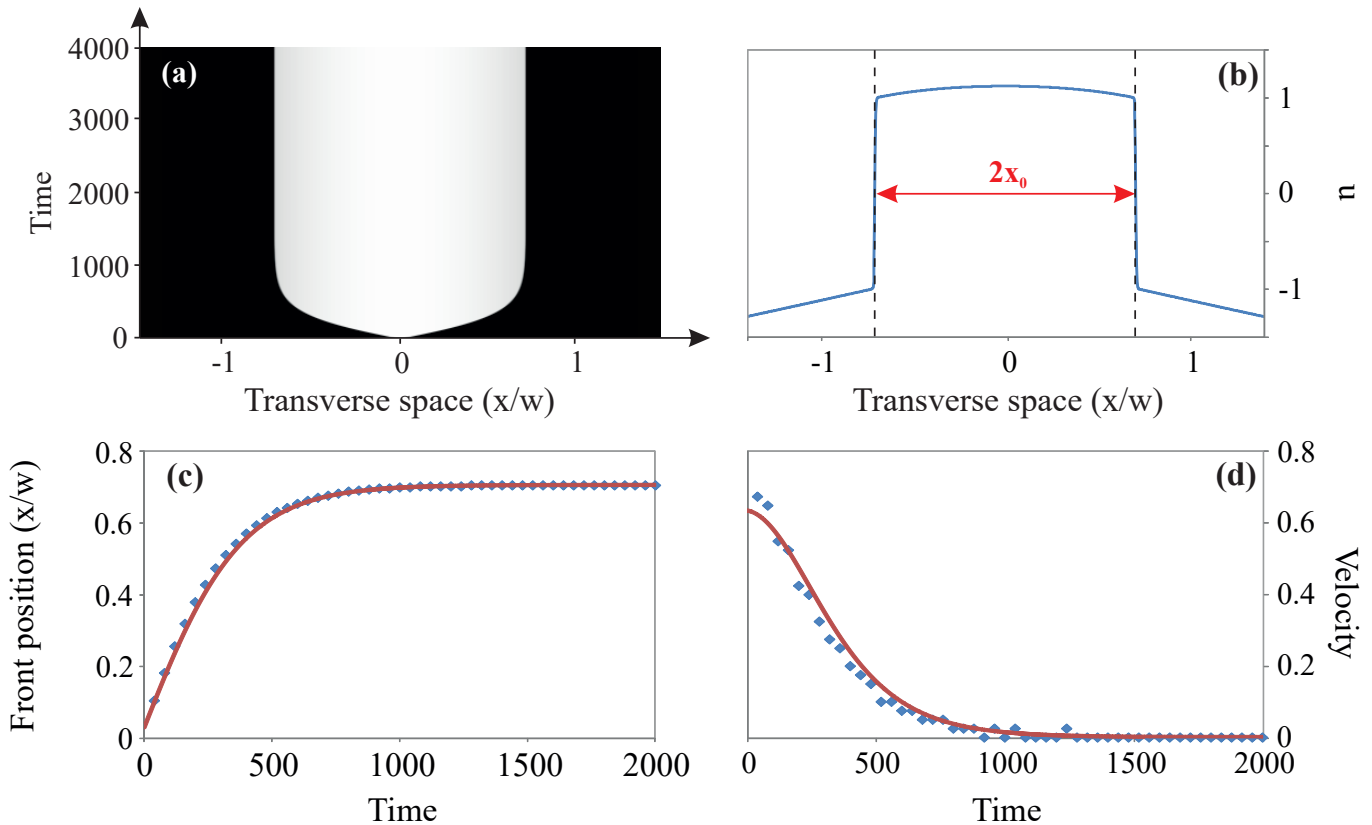


Figure 5: Numerical study of front pinning with a parabolic forcing. (a) Spatiotemporal diagram; (b) Transverse profile of the front at $t = 4000$; (c) Relative front position $x_0(t)$ (for $x > 0$); (d) front velocity. Blue diamonds are the numerical points and the red curves are the analytical predictions. $\eta_0 = 0.6$, $\tilde{\eta} = 0.3$, $w = 350$.

The ordinary differential equation (11) admits an exact solution that leads to the following trajectory of the front

$$x_0(t) = \pm a \tanh(b(t - t_0)), \quad (14)$$

with \underline{a} , \underline{b} and t_0 are coefficients depending on η_0 , $\tilde{\eta}$ and w . The equilibrium position of the front $x_{0\infty}$ can be inferred from expression Eq. (14) for $t \rightarrow \infty$ as $x_{0\infty} = \pm w \sqrt{1 - \tilde{\eta}/\eta_0}$. This equilibrium positions could be obtained directly from Eq. (7), assuming $\eta(x_{0\infty}) = 0$ which is the condition for motionless front (Maxwell point). Extending this last property to the initial Gaussian forcing, we get

$$x_{0\infty} = \pm w \sqrt{\ln\left(\frac{\eta_0}{\tilde{\eta}}\right)}. \quad (15)$$

At leading order, Eq. (15) recover again the previous expression of $x_{0\infty}$ for the parabolic approximation of the Gaussian profile.

C. Numerical results

We conduct numerical simulations of the imperfect pitchfork bifurcation, Eq. (7-8), with a parabolic spatial injection to compare with the analytical predictions. Initially, we observe the front propagation, as the case with a plane wave. Then, the front speed decreases to become zero, around $t = 1000$, as presented on [Fig. 5(a,c,d)]. At $t = 4000$, the structure is pinned by the pump parabolic profile and presents a bistable structure with a parabolic dependance on the two states [Fig. 5(b)]. We plot on the same graph [Fig. 5(c,d)], the analytical predictions of the core front position and its speed with the numerical simulations. We have an excellent agreement between both. For the Gaussian case, which is not presented in this document, the hyperbolic tangent allows always to reproduce the front trajectory. We

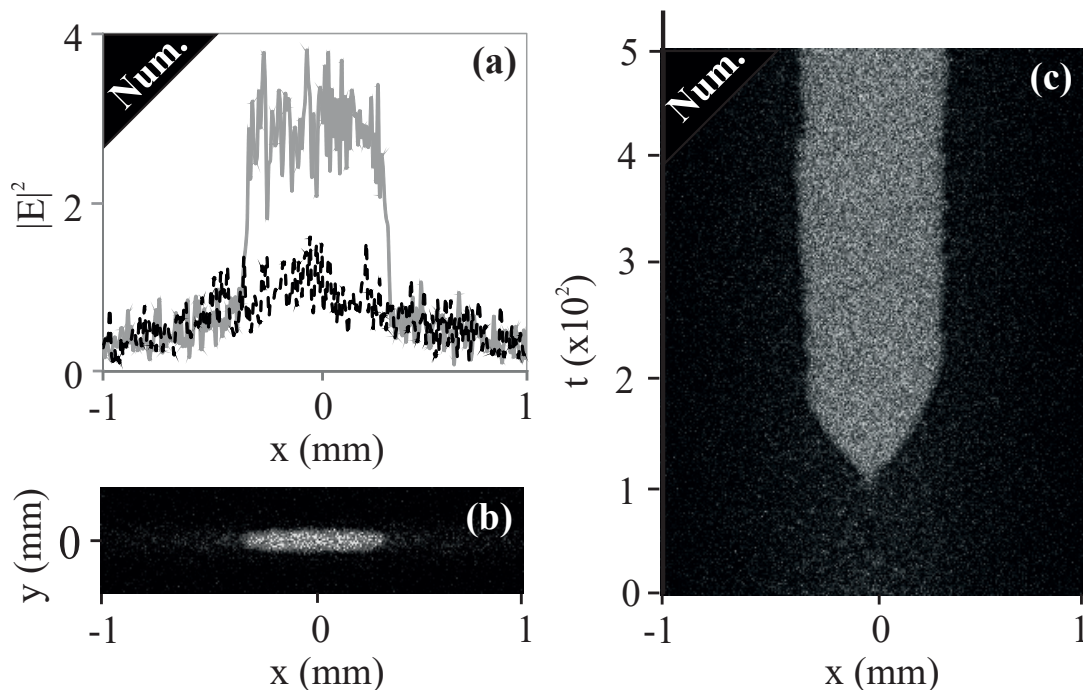


Figure 6: Front propagation in negative diffractive inhomogeneous Kerr cavity. (a,b) Transverse cross-section of the initial (final) average localized structure in dashed black line (in continue gray line). (c,d) Spatiotemporal response to a step function of the input intensity from the lower to the upper branch of the bistable cycle. (e,f) Experimental and numerical cross section of the localized state. Light region account for high intensity of the light.(a,c,e) Experiments $I_0 = 433 \text{ W.cm}^{-2}$, $d = -5 \text{ mm}$, $\varphi = -0.6 \text{ rad}$, $w_x = 1400 \mu\text{m}$, $w_y = 100 \mu\text{m}$, $R_1 = 81.8\%$; $R_2 = 81.4\%$. (b,d) Numerical simulation of LL model with $E_0 = 1.9$, $\Delta = 3.0$, $\alpha = 0.001$, $w_x = 1400 \mu\text{m}$, $w_y = 100 \mu\text{m}$, $\varepsilon = 0.4$.

need only to adjust the parameters a and b from Eq. (14) to have a good agreement between the predictions and the numerical simulations.

For the LL model, Eq. (1), we focus our numerical investigations with a bi-dimensional Gaussian spatial injection and by taking into account the experimental parameters are shown in Fig. 6.

We perform numerical simulations with a asymmetric Gaussian forcing with cigar shape ($w_x \gg w_y$)

$$E_{in}(x, y) = E_0 e^{-\left(\left(\frac{x}{w_x}\right)^2 + \left(\frac{y}{w_y}\right)^2\right)}. \quad (16)$$

Furthermore, we take account the inherent fluctuations of the system by the stochastic Lugiato-Lefever model described by Eq. 1, $\varepsilon \neq 0$. We use a stochastic Runge-Kutta solver of the order of 2 with additive noise [28]. In this latter case, the temporal step (Δt) is equal to 0.01. Numerical simulations with these ingredients show a quite good agreement with the experimental observations (see Fig. 4 and Fig. 6). Hence, the analytical expression (14) can be used to figure out and to characterize the experimental front dynamics. Figure (7) depicts the experimental and numerical temporal evolutions of the front position. It clearly evidences that the expression of Eq. (14) reproduces well the front dynamics. Therefore, the effect of a spatial forcing on front propagation is to induce the front moves and stops on an asymptotic position, satisfying a hyperbolic tangent trajectory.

IV. ZERO DIFFRACTION CAVITY

We have explored an interesting limit case, where the diffraction is zero. This limit case delimits the positive diffraction case where exists soliton solution [5, 26] and the negative diffraction, with front propagation [19]. It is natural to wonder which kind of solution exists in this limit. A linear stability study inform us that the two branch of the hysteresis cycle are linearly stable, contrary to the diffraction cases [20, 26]. Consequently, we expect to observe front solution, connecting the two branch of the bistable cycle.

The numerical simulations from Eq. (1) have been performed for a zero cavity length, i.e. zero diffraction, reveal the presence of the two states, notwithstanding without front propagation [cf. Fig. 8(a)]. However the experiments

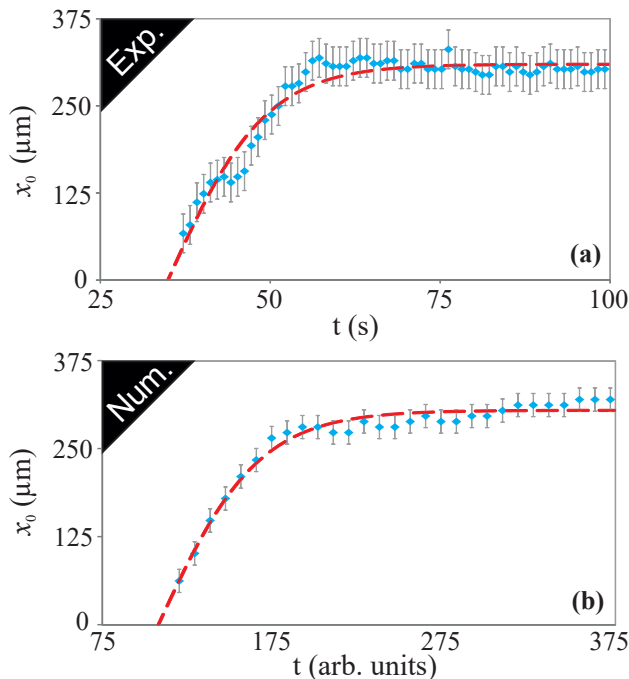


Figure 7: Temporal evolution of front position $x_0(t)$ corresponding to spatiotemporal diagrams of Fig. (4-6). (a) Experiment and (b) numerical simulations of the LL model, Eq. (1), used the same parameters considered in Fig. (4-6). Blue diamonds : location values extracted from the smoothed spatiotemporal diagrams. Dashed red curves: best fit using expression 14. Experimental fit parameters : $a = 308 \mu\text{m}$, $b = 0.069$, $t_0 = 35.2 \text{ s}$, numerical fit parameters : $a = 306 \mu\text{m}$, $b = 0.017$, $t_0 = 107.7 \text{ s}$.

realized for a zero diffraction cavity show two fronts, connecting the dark state with the bright state, with slow, asymmetric and irregular speeds [see Fig. 8(c)]. We conclude that the Lugiato-Lefever model is not enough to model the experimental observations for zero diffraction. Close to $\alpha = 0$, the diffusion of the liquid crystal molecules cannot be neglected. Consequently, we complete the model by a second equation governing the spatial nonlinear refractive index evolution. the intracavity field E and the nonlinear refractive n are given by

$$\frac{\partial E}{\partial t} = E_{in}(x) - (1 + i\Delta)E + inE - i|\alpha| \frac{\partial^2 E}{\partial r^2} + \sqrt{\varepsilon}\xi(x, t), \quad (17)$$

$$n - \sigma \frac{\partial^2 n}{\partial r^2} = |E|^2, \quad (18)$$

where σ is the diffusion coefficient. The stochastic numerical simulations realized with this model show a good agreement with the experimental observations, as presented on Fig. 8.

V. CONCLUSION

We have investigated the formation of localized structures in the Lugiato-Lefever equation in a negative diffraction regime with an inhomogeneous injected beam. We first show how to generate an equivalent left-handed Kerr material in the visible range. Experimentally, we show that the nonlinear dynamical states appearing in a focusing Kerr Fabry-Perot cavity submitted to negative optical feedback are propagating fronts in inhomogeneous medium.

We have performed a reduction of the Lugiato-Lefever equation to a simple bistable model with inhomogeneous injected beam. From this simple model we have derived a simple expression for the speed front. We have used the inhomogeneous spatial pumping in the form of Gaussian beam. The front moves and stops on a asymptotic position. The experimental trajectory of the front position under that forcing follows an hyperbolic tangent law that fully agrees with the prediction from a generic bistable imperfect pitchfork bifurcation model.

Our analysis should be applicable to all fiber resonator [25] with an inhomogeneous injected beam. In this case the coupling is provided by dispersion. When dispersion and diffraction have a comparable influence, three dimensional

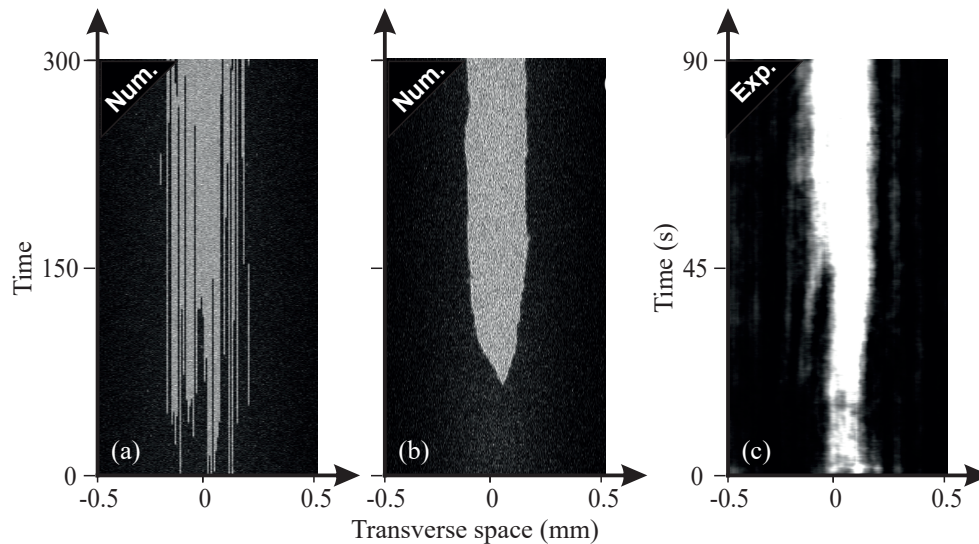


Figure 8: Spatiotemporal diagrams: (a) 1D LL model, (b) 1D LL model + liquid crystal diffusion, (c) Experiments. Experiments $I_0 = 455 \text{ W.cm}^{-2}$, $d = 0 \text{ mm}$, $\varphi = -0.6 \text{ rad}$, $w_x = 1400 \mu\text{m}$, $w_y = 100 \mu\text{m}$, $R_1 = 81.8\%$; $R_2 = 81.4\%$. Numerical simulation of LL model with $E_0 = 1.95$, $\Delta = 3.0$, $\alpha = 0$, $w_x = 1400 \mu\text{m}$, $\varepsilon = 0.4$.

localized structures can be generated [30, 31, 33–37]. These structures consist of regular 3D lattices or localized bright light bullet traveling at the group velocity of light in the material. We plan to extend our analysis to three dimensional cavities with an inhomogeneous injected beam. In this case, localized light bullet in the negative diffraction and in anomalous dispersion may be stable.

The authors acknowledge financial support by the ANR International program, project no. ANR- 2010-INTB-402-02 (ANRCONICYT39), ‘COLORS’. M. G. thanks for the financial support of FONDECYT project 1150507. This research was also supported in part by the Centre National de la Recherche Scientifique (CNRS), the ‘Fonds Européen de Développement Economique de Régions’ and by the Interuniversity Attraction 463 Poles program of the Belgian Science Policy Office, under 464 Grant No. IAP P7-35 Photonics@be.

-
- [1] H Leblond and D Mihalache, *Physics Reports*, **523**, 61 (2013).
 - [2] M. Tlidi, K. Staliunas, K. Panajotov, A.G. Vladimirov, and M. Clerc, *Localized structures in dissipative media: From Optics to Plant Ecology*, *Phil. Trans. R. Soc. A*, **372**, 20140101 (2014).
 - [3] *Localized states in physics: solitons and patterns*, editors Descalzi, O., Clerc, M., Residori, S., and Assanto, G. (Springer Science & Business Media 2011).
 - [4] A.J. Scroggie et al., *Chaos, Solitons and Fractals* **4**, 1323 (1994).
 - [5] V. Odent, M. Taki, and E. Louvergneaux, *New J. Phys.* **13**, 113026 (2011).
 - [6] Y. Pomeau, *Physica D* **23**, 3 (1986); M. Tlidi, P. Mandel, and R. Lefever, *Phys. Rev. Lett.* **73**, 640 (1994); P. Couillet, C. Riera, and C. Tresser, *Prog. Theor. Phys. Supp.* **139**, (2000); M.G. Clerc and C. Falcon, *Physica A* **356**, 48 (2005); U. Bortolozzo, M. G. Clerc, C. Falcon, S. Residori, and R. Rojas, *Phys. Rev. Lett.* **96**, 214501 (2006); M. G. Clerc, E. Tirapegui, and M. Trejo, *Phys. Rev. Lett.* **97**, 176102 (2006); A.G. Vladimirov et al., *Optics express* **14**, 1 (2006); M. Tlidi and L. Gelens, *Opt. Lett.* **35**, 306 (2010); A.G. Vladimirov et al., *Phys. Rev. A* **84**, 043848 (2011); E. Averlant, M. Tlidi, H. Thienpont, T. Ackemann, K. Panajotov, *Optics Express*, **22**, 483 (2014); V. Skarka, N. B. Aleksic, M. Lekic, B. N. Aleksic, B. A. Malomed, D. Mihalache, and H. Leblond, *Phys. Rev. A* **90**, 023845 (2014).
 - [7] K. Staliunas and V.J. Sanchez-Morcillo, *Physics Letters A* **241**, 28 (1998); M. Tlidi, P. Mandel, R. Lefever, *Phys. Rev. Lett.* **81**, 979 (1998); H. Calisto, M. Clerc, R. Rojas, E. Tirapegui, *Phys. Rev. Lett.* **85**, 3805 (2000); M. Tlidi, P. Mandel, M. Le Berre, E. Ressayre, A. Tallet, and L. Di Menza, *Opt. Lett.* **25**, 487 (2000); D. Gomila, P. Colet, G. L. Oppo, and M. San Miguel, *Phys. Rev. Lett.* **87**, 194101 (2001); C. Chevillard, M. Clerc, P. Couillet, and J.-M. Gilli, *Europhys. Lett.* **58**, 686 (2002).
 - [8] L. Pismen, *Vortices in nonlinear fields: from liquid crystals to superfluids, from non-equilibrium patterns to cosmic strings*, Clarendon Press (Oxford and New York, 1999).
 - [9] J. S. Langer, *Rev. Mod. Phys.* **52**, 1 (1980).
 - [10] P. Collet and J. P. Eckmann, *Instabilities and Fronts in Extended Systems* (Princeton University Press, Princeton, NJ, 1990).

- [11] W. van Saarloos and P. C. Hohenberg, *Physica D* **56**, 303 (1992)
- [12] P. Couillet, *Int. J. of Bifurcation and Chaos*, **12**, 2445 (2002).
- [13] J.D. Murray, *Mathematical Biology*, 3de ed. (Springer, Berlin, 2003).
- [14] R. A. Fisher, *Ann. Eugen.* **7**, 355 (1937).
- [15] A. Kolmogorov, I. Petrovsky, and N. Piskunov, *Bull. Univ. Moskou Ser. Int. Se. A* **1**, 1 (1937).
- [16] W. Van Saarloos, *Physics Reports*, **386**, 29 (2003).
- [17] Clerc M.G., Nagaya T., Petrossian A., Residori S., and Riera C., *Eur. Phys. J. D* **28**, 435-445 (2004).
- [18] R. E. Goldstein, G. H. Gunaratne, L. Gil, and P. Couillet, *Phys. Rev. A* **43**, 6700 (1991).
- [19] V. Odent, M. Tlidi, M. G. Clerc, P. Glorieux, and E. Louvergneaux *Phys. Rev. A* **90**, 011806(R) (2014).
- [20] P. Kockaert, P. Tassin, G. Van der Sande, I. Veretennicoff, and M. Tlidi, *Phys. Rev. A* **74**, 033822 (2006).
- [21] P. Tassin, G. V. der Sande, N. Veretenov, P.Kockaert, I. Veretennico, and M. Tlidi, *Opt. Express* **14**, 9338 (2006).
- [22] P. Tassin, L. Gelens, J. Danckaert, I. Veretennicoff, G. Van der Sande, P. Kockaert, and M. Tlidi, *Chaos* **17**, 037116 (2007).
- [23] A. Boardman, M. Brongersma, M. Stockman, and M. Wegener, *J. Opt. Soc. Am. B* **377**, 2009 (2009).
- [24] M. Tlidi, P. Kockaert, and L. Gelens, *Phys. Rev. A* **84**, 013807 (2011).
- [25] S. Coen, M. Tlidi, P. Emplit, and M. Haelterman, *Phys. Rev. Lett.* **83**, 2328 (1999).
- [26] L. A. Lugiato and R. Lefever, *Phys. Rev. Lett.* **58**, 2209 (1987).
- [27] G. Agez, P. Glorieux, C. Szwarz, and E. Louvergneaux, *Opt. Commun.* **245**, 243 (2005).
- [28] R. L. Honeycutt, *Phys. Rev. A* **45**, 600 (1992).
- [29] M Tlidi, M Haelterman, P Mandel *EPL (Europhysics Letters)* **42** , 505 (1998).
- [30] Tlidi, M., Haelterman, M. Mandel, *P. Quantum and Semiclassical Optics: Journal of the European Optical Society Part B* **10**, 869 (1998).
- [31] Staliunas, K., 1998 *Phys. Rev. Lett.* **81**, 81 (1998).
- [32] M. Tlidi and Paul Mandel *Phys. Rev. Lett.* **83**, 4995 (1999).
- [33] Tlidi, M., *Journal of Optics B: Quantum and Semiclassical Optics* **2**, 438 (2000).
- [34] Tassin, P., der Sande, G. V., Veretenov, N., Kockaert, P., Veretennicoff, I. Tlidi, M., *Opt. Express* **14**, 9338 (2006).
- [35] Veretenov, N. Tlidi, M., *Phys. Rev. A* **80**, 023822 (2009).
- [36] Brambilla, M., Maggipinto, T., Patera, G. Columbo, L., *Phys. Rev. Lett.* **93**, 203901 (2004).
- [37] Dai, C.-Q., Wang, X.-G. Zhou, G.-Q., *Phys. Rev. A* **89**, 013834 (2014).